

Phonons in an Inhomogeneous Continuum: Vibrations of an Embedded Nanoparticle

Daniel B. Murray¹ and Lucien Saviot²

¹*Department of Physics and Astronomy, Okanagan University College,
3333 College Way, Kelowna, British Columbia, Canada V1V 1V7**

²*Laboratoire de Recherche sur la Réactivité des Solides, UMR 5613 CNRS - Université de Bourgogne
9 avenue A. Savary, BP 47870 - 21078 Dijon - France[†]*

(Dated: February 7, 2020)

The spectrum of acoustic vibrational modes of an inhomogeneous elastic continuum are analyzed with application to a spherical nanoparticle embedded in an infinite glass block. The relationship of these modes to the discrete vibrational spectrum of a free sphere is studied. The vibrational modes of a sphere with a fixed surface are relevant in some situations. Comparisons are also made to calculations of mode frequency and damping based on complex valued frequency.

PACS numbers: 62.25.+g,63.22.+m,78.30.-j,43.20.Ks

I. INTRODUCTION

In 1882, Lamb¹ calculated the frequencies of vibration of a free isotropic homogeneous continuous sphere. Twenty years ago^{2,3}, this model was applied to nearly spherical atomic clusters a few nanometers in size (nanoparticles), whose vibrations can be observed by low frequency inelastic light scattering (Raman or Brillouin^{4,5} setups depending on the actual particle size) and also by femtosecond pump-probe experiments⁶. However, with exceptions^{5,7,8,9,10}, the free sphere model hardly seems applicable because the samples investigated are doped glasses, *i.e.* nanoparticles solidly embedded within a glass matrix.

Variations on Lamb's calculation attempt to take into account the mechanical properties of the matrix. The nanoparticle surface can be rigidly fixed¹¹. Assuming outgoing travelling waves in the matrix, complex valued mode frequencies can be found^{12,13}. These approaches give discrete sets of vibrational modes, unlike a macroscopic object in which there is a continuum.

Conversely, the nanoparticle-matrix interface influence on vibrations can be ignored¹⁴ and bulk phonon modes can be used as if the nanoparticle surface were acoustically invisible. This latter approach can be workable when other mechanisms, such as size quantization of nanoparticle electron energy levels (excitons), provide the dominant contribution to the qualitative features of light scattering spectra.

None of the foregoing provides a satisfactory description of a nanoparticle-matrix system even if they can provide valuable insight. What is needed is a calculation that properly models the effect of the presence of the nanoparticle on the phonon modes. In this paper, we present such an approach based on recent calculations on core-shell systems¹⁵.

Apart from some general observations made in section II, the nanoparticle is idealized as an isolated spherical homogeneous isotropic classical continuum object embedded in similarly idealized glass. Departures from this won't be addressed in this paper even though they can be

experimentally important. Taking into account nanoparticle size distribution is straightforward. Anisotropy has been discussed in a previous paper¹³, and here we use directionally averaged sound speeds. Non-sphericity is a more complex problem but arbitrary shapes can be investigated using molecular dynamics simulation¹³. Application of continuum elastic boundary conditions at the interface between nanoparticle and matrix is also an idealization that needs to be justified with attention to details at the microscopic level. For example, such conditions are generally incorrect for epitaxial interfaces¹⁶.

Mode frequencies predicted for a free sphere correspond to damped motions at the same frequency of the nanoparticle in a sufficiently soft and light matrix. Some qualitatively new modes appear corresponding to semi-rigid libration (angular oscillation) and rattling (translational oscillation) of the nanoparticle as a result of the elastic restoring force provided by the matrix. Mode frequencies for a sphere with a fixed boundary correspond to the damped motions of a nanoparticle in a harder and denser matrix.

II. GENERAL INHOMOGENEOUS SYSTEM

Consider a continuous elastic medium which may be inhomogeneous and anisotropic. $\vec{r}(\vec{R}, t)$ denotes real space coordinates of the point of matter which has material coordinate \vec{R} . Deviation from equilibrium is described in terms of the displacement field $\vec{u}(\vec{R}, t) = \vec{r}(\vec{R}, t) - \vec{R}$. The mass density of the medium is $\rho(\vec{R})$. Note that this density refers to material coordinates. The density in real space coordinates varies as acoustic vibrations in the medium cause local expansion and contraction.

The elastic constants of the material are $c_{ijkl}(\vec{R})$. Stress is related to the displacement field through $\sigma_{ij} = c_{ijkl}u_{k,l}$ where a summation is implied over repeated indices and the comma implies a partial derivative. The equation of motion is $\rho(\vec{R})\ddot{u}_i = \sigma_{ij,j}$.

In the formalism used here, $\vec{u}(\vec{R}, t)$ is real valued. The equation of motion has normal modes $\vec{u}_j(\vec{R})$ with fre-

frequency ω_j where j is a mode index. The angular frequency ω (in rad/s) is related to the wavenumber ν (in cm^{-1}) through $\nu = \omega/(200\pi c)$ where c is the speed of light (in m/s). Modes are orthonormalized using

$$\int \rho(\vec{R}) \vec{u}_i(\vec{R}) \cdot \vec{u}_j(\vec{R}) d^3 R = \delta_{ij} M_{p+m} \quad (1)$$

for any two modes i and j , where M_{p+m} is the mass of the system (nanoparticle and matrix). The integration is over the volume of the system. Equation (1) is justified in Appendix A. A general disturbance of the system has displacement field

$$\vec{u}(\vec{R}, t) = \sum_j (x_j \sin(\omega_j t) + y_j \cos(\omega_j t)) \vec{u}_j(\vec{R}) \quad (2)$$

On the basis of the normalization chosen, $\vec{u}_j(\vec{R})$ is dimensionless. Therefore x_j and y_j have units of metres.

Inserting (2) into (A1) and (A2) and simplifying using (A7) and (A8), the total energy of the system is

$$E = \frac{1}{2} M_{p+m} \sum_j \omega_j^2 (x_j^2 + y_j^2) \quad (3)$$

III. SPHERICALLY SYMMETRIC MODELS

In this and later sections the displacement field depends on spherical material coordinates $\vec{R} = (R, \theta, \phi)$. The nanoparticle ("p") is idealized as a homogeneous and isotropic sphere of radius R_p and density ρ_p with speeds of sound v_p^L and v_p^T .

In the free sphere model¹ (FSM), zero traction force (*i.e.* $\sigma_{ij} n_j = 0$ where \hat{n} is the unit surface normal) boundary conditions are applied for all θ and ϕ at $R = R_p$. Mode frequencies are $\omega_{lmnq}^{\text{FSM}}$ where q can be spheroidal (SPH) or torsional (TOR), l and m are angular momentum and its z-component, and n is the harmonic index. For convenience, these modes will be called "pseudomodes" when referring to situations of a sphere that is only weakly coupled to its surroundings.

In the bound sphere model¹¹ (BSM), zero displacement boundary conditions apply for all θ and ϕ at $R = R_p$. Mode frequencies are $\omega_{lmnq}^{\text{BSM}}$.

In the complex frequency model^{12,13} (CFM), the nanoparticle is surrounded by a homogeneous and isotropic matrix ("m") of density ρ_m and speeds of sound v_m^L and v_m^T . The matrix extends to infinity. Continuity of \vec{u} and force-balance apply at the nanoparticle-matrix interface. The boundary condition at large R is that \vec{u} is an outgoing travelling wave. The mode frequencies $\omega_{lmnq}^{\text{CFM}}$ are complex valued. In spectroscopic observations of such a mode (a plot of scattered light intensity versus wavenumber ν) a broadened peak is observed with its center at $\nu = \text{Re}(\omega)/(200\pi c)$ and with a half width at half maximum (HWHM) of $\text{Im}(\omega)/(200\pi c)$.

nanoparticle matrix	none	normal	rigid heavy
none	FSM		
normal	VCFM	CFM, CSM	RCFM
rigid heavy	BSM		
	FSM	Free Sphere Model	
	BSM	Bound Sphere Model	
	CFM	Complex Frequency Model	
	RCFM	Rigid CFM	
	VCFM	Void CFM	
	CSM	Core-Shell Model	

TABLE I: Acronyms used throughout this paper.

There are two important limiting cases of CFM: In the rigid complex frequency method (RCFM) the nanoparticle is made infinitely rigid and heavy. In the void complex frequency method (VCFM) the nanoparticle is replaced by an empty void.

CFM, RCFM and VCFM necessarily have complex-valued \vec{u} which blows up exponentially with R and cannot be orthonormalized. Equations (1) to (4) and the discussion in the appendices are for FSM, BSM and CSM only and do not apply to CFM, RCFM and VCFM.

IV. CORE-SHELL MODEL

Adapting the core-shell model (CSM) developed for Ni-Ag nanoparticles¹⁵ we consider a nanoparticle as in the previous section concentrically within a much larger homogeneous and isotropic sphere (representing the glass matrix) with radius R_m . In the macroscopic limit R_m goes to infinity, and the frequency of every vibrational mode varies as $1/R_m$ and therefore goes to zero. Going from the FSM to an embedded sphere with a macroscopic matrix means changing from a discrete set of vibrational modes to a continuum.

We are primarily interested in inelastic light scattering situations (Raman or Brillouin) in which light is scattered from the nanoparticle rather than from the transparent matrix material. Low frequency vibrations of the nanoparticle allow the scattered photon to have wavenumber a few cm^{-1} above or below those in the incident laser beam. The general idea behind this core-shell approach is that although the vibrations of the whole system are described by a continuum of modes, the nanoparticle doesn't move as much for matrix phonons of certain wavelengths.

The inelastically scattered light is modulated by the frequency-dependent amplitude of the vibration within the nanoparticle. The mechanism for the photon scattering process depends on the electronic details of the nanoparticle: In semiconductors, bound excitons; In metals, resonant plasmons; In insulators, strain-optic coupling. In any case, a preliminary step is to study the amplitude of nanoparticle vibrations as a function of phonon

frequency. That is the goal of our present investigation.

The first step is to solve the equation of motion for a given value of R_m . Extending Takagahara's work¹⁷ to core-shell systems, the normal modes have displacement fields \vec{u}_{lmnq} which are normalized with respect to Eq. (1). Orthogonality of the modes was also checked numerically.

For the results reported here, the outer surface of the matrix has zero traction force boundary conditions.

To compare CSM with the FSM, BSM and CFM models, we compare the discrete frequency sets to the position and width of peaks of the mean square displacement inside the nanoparticle (Eq. (4) where \vec{u}_{lmnq} is obtained from CSM) as a function of frequency.

$$\langle u_{lmnq}^2 \rangle_p = \int_{R < R_p} \|\vec{u}_{lmnq}(\vec{R})\|^2 d^3 \vec{R} \quad (4)$$

Using the selection rules predicted by Duval¹⁸, one can get a rough idea of what the reduced Raman spectrum might look like: only (SPH, $l=0$) and (SPH, $l=2$) modes are Raman active for a spherical isotropic nanoparticle under non-resonant excitation.

The mean square displacement $\langle u^2 \rangle_p$ that we plot in our figures is only one of many possible measures of the internal motion of the nanoparticle. If we are interested in low-frequency inelastic light scattering, then ultimately we want to calculate the scattered photon spectrum. Our model provides a key ingredient for such a calculation in the $\vec{u}_{lmnq}(\vec{R})$. Just as in plane wave vibrational modes, second quantization can be applied to these modes to obtain phonon creation and annihilation operators¹⁷ which would be required in any model of photon scattering.

The issue of choosing the matrix radius R_m turns out to be easy to solve. The $\langle u^2 \rangle_p$ variation with the mode frequency is not affected by the R_m/R_p ratio provided this ratio exceeds several times unity. Increasing this ratio results in more vibrational modes for a given frequency range. This increase is compensated by the lower amplitude associated with each mode. In this paper, we use $R_m/R_p = 100$ when possible to have enough modes and better looking plots. Calculations with bigger ratios were performed but don't change the results. Please note that $R_m/R_p = 100$ means that the nanoparticle occupies $1/1000000^{\text{th}}$ of the total volume.

V. DISCUSSION

A. Ag in BaO-P₂O₅ glass

Low-frequency inelastic light scattering¹⁹ and femtosecond pump-probe experiments⁶ on nearly spherical Ag nanoparticles grown in a BaO-P₂O₅ (high density glass) matrix show very well resolved features, making it a perfect system to start with.

Elastic parameters for silver at 300K²⁰ are directionally averaged¹³ giving sound speeds 1740 m/s and 3750

q	l	n	FSM	CFM		RCFM	
			ν	ν	$\Delta\nu$	ν	$\Delta\nu$
TOR	2	0		2.6	5.8	2.4	4.2
		1	4.7	7.2	1.0		
		2	13.5	13.9	1.1		
		3	19.8	20.1	1.1		
		4	26.0	26.2	1.1		
TOR	1	0		4.9	1.1		
		1	10.9	11.4	1.1		
		2	17.1	17.5	1.1		
		3	23.2	23.5	1.1		
		4	29.2	29.4	1.1		
SPH	2	0	5.0	5.8	1.4	8.2	7.5
		1		8.8	9.2		
		2	9.7	11.1	1.2		
		3	16.4	17.0	1.1		
		4	21.9	22.4	1.6		
		5	23.6	23.5	1.5		
		6	29.0	29.2	1.1		
SPH	1	0		2.9	1.5	4.1	6.4
		1		4.5	8.0		
		2	6.9	8.4	1.2		
		3	13.8	14.3	1.1		
		4	17.3	17.6	1.9		
		5	20.3	20.5	1.2		
		6	26.2	26.4	1.1		
SPH	0	0	11.4	11.9	1.9		
		1	24.9	25.1	1.9		

TABLE II: Wavenumber (ν) and HWHM damping ($\Delta\nu$) in cm^{-1} for free (FSM), BaO-P₂O₅ embedded Ag nanoparticles (CFM) and rigid nanoparticle (RCFM) for modes with $\nu < 30 \text{ cm}^{-1}$ and $R_p = 4.9 \text{ nm}$.

m/s. The actual transverse speed of sound in Ag varies from 1195 m/s to 2080 m/s depending on the direction. Longitudinal speed of sound varies from 3410 to 3935 m/s. Rms averaged speeds (1760 m/s, 3750 m/s) are comparable to the average speeds. FSM vibrational frequencies calculated using directionally averaged speeds are in good agreement with frequencies calculated with a molecular dynamic approach which fully takes into account elastic anisotropy.¹³ Mass density and sound speeds for the BaO-P₂O₅ matrix are taken from Voisin *et al.*⁶.

Table II shows FSM, CFM and RCFM wavenumbers and HWHM damping. As already reported for silicon nanoparticles inside silica¹³, there is good agreement between the CFM and FSM approaches. The main differences of CFM are: (1) nonzero damping and (2) "extra modes" as described in the following section. RCFM modes match some of the CFM modes not predicted by FSM.

To present CSM results, the measure of nanoparticle motion in Figs. 1 to 5 is $\langle u^2 \rangle_p$, the mean squared displacement within the nanoparticle of the normalized vibrational mode displacement field as calculated using Eq. (4). In each case, $\langle u^2 \rangle_p$ is plotted individually for each mode versus the mode's wavenumber in cm^{-1} . To make it easier to compare different materials and differ-

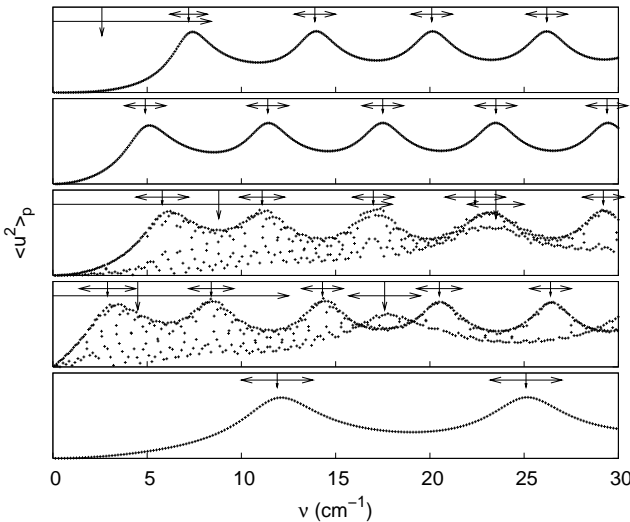


FIG. 1: Mean square displacement within the nanoparticle interior of vibrational modes for Ag $R_p=4.9$ nm in BaO-P₂O₅ with $R_m/R_p = 100$. SPH $l=0,1$ and 2 and TOR $l=1$ and 2 from bottom to top. Arrows indicate positions and FWHM obtained with the CFM.

ent sizes, the different $\langle u^2 \rangle_p$ plots cover approximately the first two (SPH, $l=0$) pseudomodes.

Figure 1 shows individual plots for the separate cases of q and l . Wavenumbers and HWHM of pseudomodes using CFM as listed in Tab. II are also indicated on the figure as arrows.

It is apparent that the interior of the nanoparticle is in motion for every CSM mode, unlike FSM wherein the nanoparticle would only vibrate at a discrete set of frequencies.

Relatively smooth dependence of $\langle u^2 \rangle_p$ on frequency is seen for (TOR, $l=1$), (TOR, $l=2$) and (SPH, $l=0$) modes. The graph is much more complicated for the (SPH, $l=1$) and (SPH, $l=2$) cases. In these latter spheroidal modes, the motion is a mixture of longitudinal and transverse waves travelling at different speeds. Normal modes are forced to mix these two polarizations in order to satisfy zero traction boundary conditions at $R = R_m$.

Points in the (SPH, $l \neq 0$) plots clearly tend to cluster on two curves, with a few points lying in between. The (SPH, $l \neq 0$) plots consist of a longitudinal-like curve with one broad peak and a transverse-like curve with five peaks. CFM calculations also reveal this feature because some modes are broader.

In agreement with Voisin *et al.*⁶, Fig. 1 shows that Ag in BaO-P₂O₅ has significant damping, but the nanoparticle's damped pseudomodes are clearly visible. This probably explains why well resolved Raman peaks can be observed¹⁹.

With the exception of "matrix modes" discussed in the following section, there is good agreement between the maxima of $\langle u^2 \rangle_p$ from CSM and the wavenumbers and HWHM as predicted using CFM. Where CFM pre-

dicts modes where no $\langle u^2 \rangle_p$ peaks appear, these also correspond to RCFM modes as discussed below. This and subsequent figures demonstrate the utility of CFM to predict the dominant frequencies at which the nanoparticle oscillates as well as their width.

B. Extra Modes

The presence of the matrix leads to the appearance of some qualitatively new modes not given by FSM. We classify these as: (1) semi-rigid librational modes, which appear at the low frequency end of the (TOR, $l=1$) plots (near 5 cm⁻¹ in Fig. 1). Both CFM and CSM confirm their presence. The zero frequency limit of FSM for (TOR, $l=1$) corresponds to rigid rotation. We therefore identify low frequency (TOR, $l=1$) modes as nearly rigid rotational oscillation. (2) semi-rigid rattling modes, also at the low frequency end of the (SPH, $l=1$) plots (near 3 cm⁻¹ in Fig. 1), also confirmed by both CFM and CSM. The zero frequency limit of FSM for (SPH, $l=1$) corresponds to rigid rectilinear motion. We therefore identify low frequency (SPH, $l=1$) modes as nearly rigid translational oscillation. (3) "matrix modes" predicted by CFM but not apparent in the plots of $\langle u^2 \rangle_p$ from CSM. These modes are well approximated by RCFM, which confirms their nature as motions of the matrix which do not significantly shake the nanoparticle.

As an example of a "matrix mode", the lowest (TOR, $l=2, n=0$) mode in Fig. 1 at 2.6 cm⁻¹ as calculated using the CFM does not correspond to a CSM peak in $\langle u^2 \rangle_p$. The frequency and width of this mode is insensitive to the hardness and density of the nanoparticle in the CFM calculation and therefore the motion is primarily confined to the matrix. These are also close to the RCFM (TOR, $l=2$) frequency and HWHM (see Tab. II) of a BaO-P₂O₅ matrix with a 4.9 nm hole in it with a "rigid boundary" condition which represents a matrix embedding an infinitely heavy and rigid nanoparticle.

Similar arguments apply to CFM (SPH, $l=1, n=1$) and (SPH, $l=2, n=1$) "matrix modes" of the nanoparticle-matrix system which correspond to the RCFM (SPH, $l=1$) and (SPH, $l=2$) modes of the matrix given in Tab. II. From Eq. (4), displacement within the matrix has no influence on $\langle u^2 \rangle_p$. Since they do not shake the nanoparticle, these "matrix modes" are therefore not likely to be seen in Raman scattering experiments.

C. Pseudomode Damping

In the absence of the matrix, the nanoparticle will vibrate at frequencies ω_{lmnq}^{FSM} . Coupling of the nanoparticle to the matrix damps these pseudomodes.

One way to get a qualitative feeling for this problem is to compare acoustic impedances. In a fluid, acoustic impedance is density times speed of sound. For pressure waves in fluids, reflection at normal incidence from

a planar interface is related to the difference of acoustic impedance between the two fluids. This concept also applies in general terms to acoustic waves in a solid. When acoustic impedances for the nanoparticle $Z_p = \rho_p v_p^L$ and the matrix $Z_m = \rho_m v_m^L$ match, reflection of longitudinal sound waves is negligible. Some revision of this simple picture is needed since the nanoparticle-matrix interface is non-planar as discussed in Appendix D.

As the acoustic impedance mismatch increases, acoustic wave reflection increases leading to more pronounced nanoparticle modes. This is clearly seen in Fig. 2 where varying only the density of the matrix changes the locations of frequencies at which $\langle u^2 \rangle_p$ peaks. For low matrix mass density ($Z_p > Z_m$), $\langle u^2 \rangle_p$ peaks close to the FSM frequencies. For high matrix mass density ($Z_p < Z_m$), peaks appear close to the BSM frequencies. For matching impedances ($\rho_m \approx 2.24\rho_{\text{BaO-P}_2\text{O}_5}$), oscillations are weak.

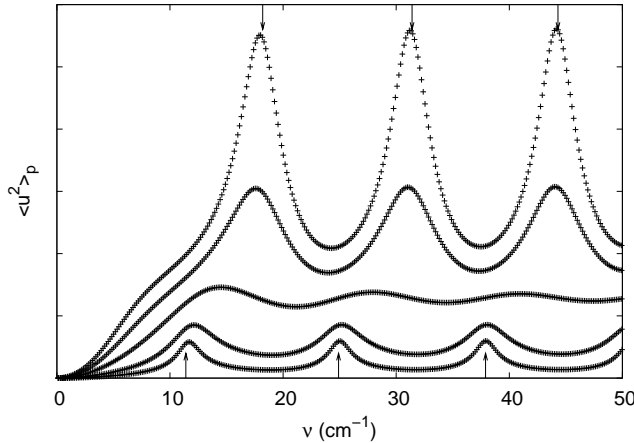


FIG. 2: Mean square displacement within the nanoparticle interior of (SPH, $l=0$) CSM modes for a 4.9 nm radius silver particle and $R_m/R_p = 100$. Matrix sound speeds are for BaO-P₂O₅. Matrix mass density is scaled from BaO-P₂O₅ by factors of 0.5, 1, 2.24, 4 and 6 from bottom to top. Arrows indicate the vibrational wavenumbers for the same silver particle with rigid (BSM, top) and free (FSM, bottom) boundary conditions.

D. Na in BaO-P₂O₅ glass

This hypothetical case illustrates a soft nanoparticle in a hard matrix. Sodium is a very light and soft metal. BaO-P₂O₅ is a heavy and rigid kind of glass.

Elastic parameters for Na at 300 K are from P. Ho *et al.*²¹ and directionally averaged to get sound speeds 1610 m/s and 3300 m/s. In this case $Z_p/Z_m \approx 0.182$.

Figure 3 shows the plots of $\langle u^2 \rangle_p$ from CSM. CFM mode wavenumbers and HWHM are shown as arrows. Peaks of $\langle u^2 \rangle_p$ are always narrow and close to BSM frequencies (not shown). CFM predicts additional much broader peaks which do not appear in $\langle u^2 \rangle_p$, but these

TABLE III: Wavenumber (ν) and damping ($\Delta\nu$) in cm⁻¹ of modes of a BaO-P₂O₅ matrix surrounding a spherical cavity (VCFM) with radius $R_p = 4.9$ nm.

mode	l	n	VCFM	
			ν	$\Delta\nu$
SPH	0	0	4.6	3.2
		1	7.9	4.4
		2	2.9	2.3
	1	1	4.1	10.4
		2	11.9	5.0
		2	2.4	4.2
TOR	1	0	5.4	4.2

mode	l	n	SiO ₂		GeO ₂	
			ν	$\Delta\nu$	ν	$\Delta\nu$
SPH	0	0	7.6	12.2	4.4	7.0
		1	15.2	14.5	8.8	8.3
		2	5.1	8.8	2.9	5.0
TOR	1					

TABLE IV: Wavenumber (ν) and HWHM ($\Delta\nu$) in cm⁻¹ of a matrix surrounding an infinitely rigid and heavy sphere (RCFM). Sphere radius is 3.4 nm.

are close to VCFM frequencies as given in Tab. III. Unlike a heavy nanoparticle in a light matrix, no additional low frequency mode corresponding to semi-rigid librational (TOR,1) or rattling (SPH,1) mode appears in the $\langle u^2 \rangle_p$ plots.

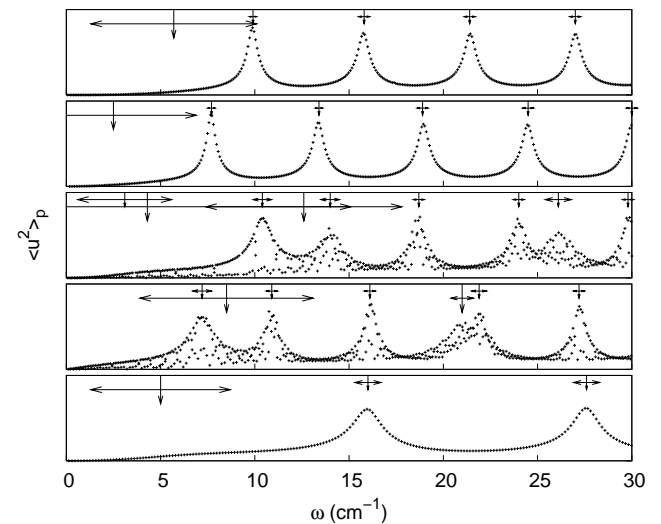


FIG. 3: Mean square displacement within the nanoparticle interior of CSM vibrational modes for Na in BaO-P₂O₅ with $R_m/R_p = 100$ and $R_p = 4.9$ nm. SPH $l=0,1$ and 2 and TOR $l=1$ and 2 from bottom to top. Arrows indicate positions and FWHM obtained from CFM.

E. Si in SiO_2

This example is chosen to show what happens when the elastic properties of the nanoparticle and the matrix are very similar. Low frequency Raman experiments on such systems^{13,22,23} reveal broad peaks whose Raman position scales inversely with nanoparticle size.

Elastic parameters and mass density for silicon and silica are taken from our previous work¹³. $R_p = 3.4 \text{ nm}$ comes from the same paper and we chose to use the same value for the following systems. In contrast to Ag in $\text{BaO-P}_2\text{O}_5$ where $Z_p/Z_m \approx 2.34$, in the case of silicon inside silica, we have $Z_p/Z_m \approx 1.60$. As can be seen in Fig. 4, this results in blurred features. Silicon has a lower sound speed ratio ($c^L/c^T \approx 1.67$) than silver (2.15). Therefore fewer TOR and (SPH, $l \neq 0$) pseudomodes are seen in the figure. In a previous work¹³, we attributed the lowest observed low-frequency inelastic light scattering peak to scattering by the first (TOR, $l=1$) pseudomode. At the same time, we pointed out that the calculated damping was too high. From the (TOR, $l=1$) plot, we can see that a proper description of the scattering process is necessary to model the Raman spectrum. In particular, the role of the electronic levels need to be taken into account. At the same time, a better description of the silicon-silica interface could somewhat mechanically isolate the silicon nanoparticle which would result in narrower pseudomodes. Introducing a thin intermediate layer between the nanoparticle and the matrix is a way to achieve this¹⁵. However, choosing the mass density and elastic parameters for this intermediate shell is a difficult task.

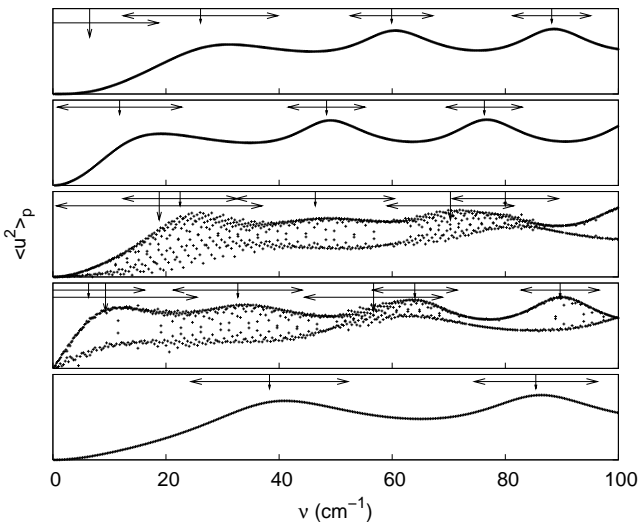


FIG. 4: Mean square displacement within the nanoparticle interior of CSM vibrational modes for Si in SiO_2 with $R_m/R_p = 100$ and $R_p = 3.4 \text{ nm}$. SPH $l=0,1$ and 2 and TOR $l=1$ and 2 from bottom to top. Arrows indicate positions and FWHM obtained from CFM.

F. CdS

Many low-frequency Raman studies have been published for matrix embedded $\text{CdS}_x\text{Se}_{1-x}$ nanoparticles. Because of the different matrices used and varying nanoparticle composition, it is very difficult to address all of them here. In this paper, we will focus on CdS nanoparticles and show the influence of two different matrices. Low-frequency Raman spectra of CdS nanoparticles embedded in sol-gel silica have been reported by Othmani *et al.*²⁴ and Saviot *et al.*²⁵. GeO_2 embedded CdS nanoparticles were investigated by Tanaka *et al.*²⁶.

Elastic parameters for CdS at 300K are taken from Berlincourt *et al.*²⁷ and directionally-averaged as before to get sound speeds 1870 m/s and 4290 m/s. We use elastic constants measured at constant electric field and do not consider piezoelectric corrections.

Mass density and sound speeds for amorphous GeO_2 are from Antoniou *et al.*²⁸.

CSM $\langle u^2 \rangle_p$ plots and CFM results are presented in Fig. 5.

In both cases $Z_p/Z_m \approx 1.6$ which is very close to the previous Si in SiO_2 system. GeO_2 having a smaller impedance than SiO_2 (even when using transverse sound speeds), one would expect the features of the GeO_2 embedded nanoparticles to be slightly more pronounced than the SiO_2 ones because the impedance mismatch is bigger. It turns out to be more complex. Modes having a strong longitudinal character follow this trend while those having a strong transverse character present more resolved low-frequency features for SiO_2 . This is revealed by both the CFM and CSM calculations. Notably, in the SiO_2 matrix, both CSM and CFM show a sharp (TOR, $l=1$) rigid librational mode at 10.3 cm^{-1} . The hexagonal crystal structure and lack of inversion symmetry of CdS makes its electronic properties anisotropic even if the nanocrystal is a perfect sphere. So it is possible that this mode could be Raman active. Acoustic properties are anisotropic too, even if this paper works around this issue by performing a directional average. Rigid librations may therefore have the ability to couple to electronic degrees of freedom and modulate inelastic light scattering.

The only satisfactory way to explain the low-frequency Raman features is to couple the CSM approach with the work done by Sirenko *et al.*¹⁴ on the interaction of the electronic excitations quantized in the confining potential of the nanoparticle with bulk-like acoustic phonons. The calculated Raman spectra should be further narrowed by taking into account the variation of the vibration amplitude inside the nanoparticle as a function of the vibration frequency.

G. Vibrational density of states

Free²⁹ and weakly coupled³⁰ nanoparticles are interesting objects because their VDOS below the lowest FSM

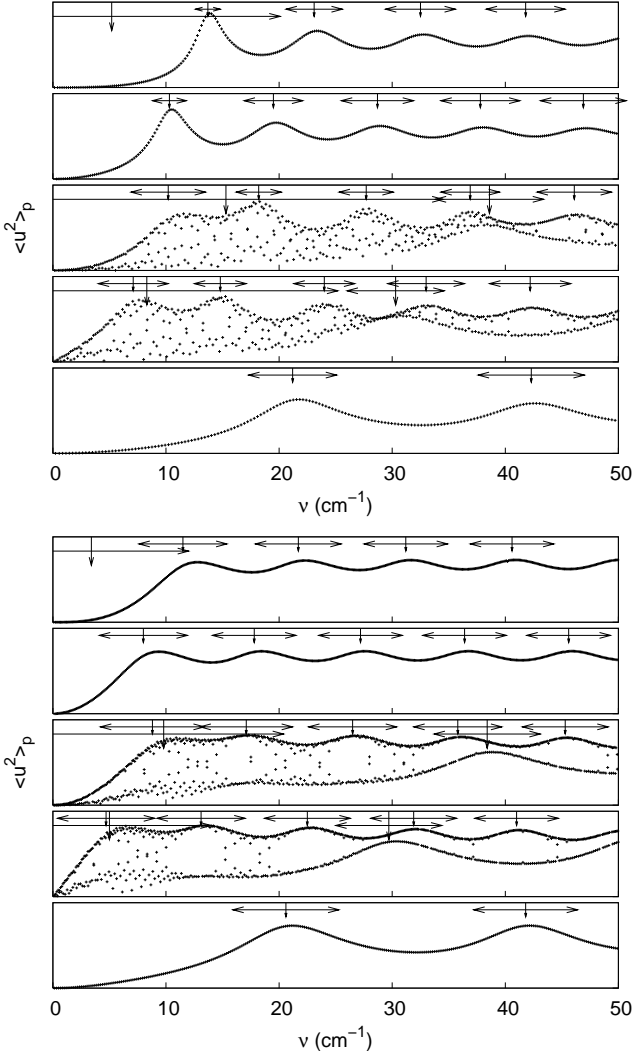


FIG. 5: Mean square displacement within the nanoparticle interior of vibrational modes for CdS in SiO₂ (top) and GeO₂ (bottom) with $R_m/R_p = 100$ and $R_p = 3.4$ nm. SPH $l=0,1$ and 2 and TOR $l=1$ and 2 from bottom to top. Arrows indicate CFM positions and FWHM.

mode vanish. However, in our case both FSM and CFM have discrete mode spectra and do not reproduce the correct phonon density of states. Using CSM we calculated the vibrational densities of states (VDOS). Note that this only involves finding the frequencies of the core-shell system. Amplitude normalization is not needed here.

$$\frac{N(\nu)}{V} = \frac{1}{V} \int_0^\nu D(\nu') d\nu' \quad (5)$$

The cumulative number of modes per unit volume up to wavenumber ν (Eq. (5)) is plotted in Fig. 6 for the case of a silver nanoparticle embedded in a BaO-P₂O₅ matrix. The lowest frequency for a given mode (q,l) increases with l . The numbers of TOR and SPH modes up to $l=60$ had to be summed taking into account the $2l+1$

degeneracy. In this way, the VDOS up to $\nu = 15$ cm⁻¹ for $R_m/R_p = 10$ was obtained. Calculations for $R_m/R_p = 3$ were also performed. Results are compared to the Debye model using matrix sound speeds (Eq. (6)).

$$\frac{N_{Debye}(\nu)}{V} = \frac{1}{2\pi^2} \left(\frac{1}{c_m^3} + \frac{2}{c_t^3} \right) \frac{\nu^3}{3} \quad (6)$$

We note that the presence of the nanoparticle doesn't appreciably modify the VDOS, even for a small matrix radius.

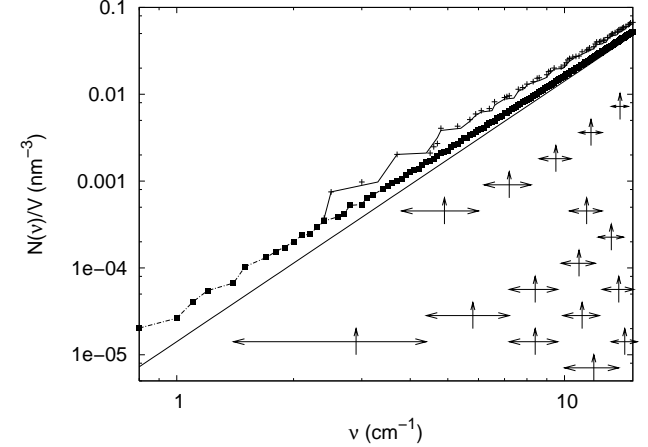


FIG. 6: Cumulative number of phonon modes per unit volume as a function of wavenumber for a silver nanoparticle inside BaO-P₂O₅ with $R_m/R_p = 3$ (plus symbols) and $R_m/R_p = 10$ (square symbols). The corresponding matrix only points are connected with lines and are very close to the previous symbols. The straight line corresponds to the Debye model (Eq. (6)). Position and width of the nanoparticle CFM pseudomodes are indicated by arrows: SPH $l=0,1,2,3,4,5$ and TOR $l=1,2,3,4,5$ from bottom to top respectively. "Matrix modes" are not shown.

VI. CONCLUSION

Within a continuum elastic approximation, the phonon spectrum of an isotropic spherical nanoparticle embedded in a macroscopic matrix can be calculated without approximation. This facilitates computations that require information about the phonon modes, and resolves the apparent contradiction involved in using free sphere vibrational modes to describe the mechanical oscillations of embedded nanoparticles.

Even though by necessity an object embedded in a macroscopic matrix must vibrate at every frequency, the vibration of a nanoparticle in a light and soft matrix is clearly dominated by FSM modes. This explains the success of FSM to reproduce the results of Raman scattering experiments on metal and semiconductor nanoparticles embedded in glasses.

CFM is demonstrated to accurately predict both the frequency and HWHM of pseudomodes of a matrix-embedded nanoparticle. New low frequency features corresponding to semi-rigid librational and rattling motions as a result of the restorative force of the matrix are clearly confirmed using both CFM and CSM. This points out the most serious limitation of FSM for embedded nanoparticles. Even so, FSM-predicted frequencies of pseudomodes turn out to be surprisingly accurate. The effect of matrix embedding is not to significantly shift nanoparticle pseudomodes but rather to dampen them. It is the acoustic impedance mismatch between nanoparticle and matrix due both to density and speed of sound difference that allows this dampening to be sufficiently slight that nanoparticles can "look free" in some light scattering experiments.

While the new (SPH, $l=1$) and (TOR, $l=1$) modes are not Raman active for an isotropic perfectly spherical nanoparticle, various imperfections can potentially allow these motions to modulate the polarizability of the nanoparticle and contribute to Raman and Brillouin spectra. However, in situations where elaboration methods allow relatively spherical nanoparticle growth, these new modes remain "invisible" in Raman and Brillouin experiments. "Matrix modes" are also present, but because they are mainly restricted to the matrix, they can't be observed in experiments which are very often made under resonant conditions on the nanoparticle electronic transitions. Thus, the new qualitative features of the motion of embedded nanoparticles are not readily observable in experiments.

Size variation within a sample of nanoparticles causes a distribution of nanoparticle pseudomode frequencies. Sample characterization methods such as TEM have the ability to measure the extent of this size variation, but elaboration methods are normally limited in their ability to restrict the range of nanoparticle radius within a sample. This important effect "masks" whatever line broadening of the pseudomodes results from matrix embedding.

Taken together, every feature of these systems conspires to obscure experimental indications that the nanoparticles really are embedded in solid material as opposed to being suspended in a vacuum. Consequently the original 1882 Lamb FSM remains a powerful calculational tool for the description of nanoparticle vibrations.

Displacement fields using CFM are complex valued and also blow up exponentially with R . Also, the frequencies are complex valued. So these cannot be used as classical degrees of freedom to be quantized. CSM provides a rigorous foundation for more detailed theoretical studies since it is clear how it can be quantized. Work is in progress to apply this approach together with the proper description of the nanoparticle confined electronic levels in order to simulate the Raman spectrum of some systems.

APPENDIX A: MODE ORTHOGONALITY

The kinetic energy of the system (assuming only mode A is excited) is:

$$T_A(t) = \int \frac{1}{2} \rho(\vec{R}) \|\dot{\vec{u}}_A(\vec{R}, t)\|^2 d^3 \vec{R} \quad (A1)$$

The elastic potential energy of mode A is:

$$V_A(t) = \int \frac{1}{2} c_{ijkl} u_{Ai,j} u_{Ak,l} d^3 \vec{R} \quad (A2)$$

The total energy of mode A is

$$E_A = T_A(t) + V_A(t) \quad (A3)$$

By conservation of energy E_A cannot depend on time. Suppose now that two modes A and B ($\omega_A \neq \omega_B$) are simultaneously excited, so that

$$\vec{u}(\vec{R}, t) = \sin(\omega_A t) \vec{u}_A(\vec{R}) + \sin(\omega_B t) \vec{u}_B(\vec{R}) \quad (A4)$$

$T_{A+B}(t)$ is the kinetic energy due to the superposition of the two modes. Therefore,

$$\begin{aligned} T_{A+B}(t) &= T_A(t) + T_B(t) \\ &+ \omega_A \omega_B \cos(\omega_A t) \cos(\omega_B t) \int \rho \vec{u}_A \cdot \vec{u}_B d^3 \vec{R} \end{aligned} \quad (A5)$$

$V_{A+B}(t)$ is the elastic potential energy due to the superposition of the two modes. So,

$$\begin{aligned} V_{A+B}(t) &= V_A(t) + V_B(t) \\ &+ \sin(\omega_A t) \sin(\omega_B t) \int c_{ijkl} u_{Ai,j} u_{Bk,l} d^3 \vec{R} \end{aligned} \quad (A6)$$

With both modes excited, the energy is E_{A+B} . Based on the above we can evaluate $E_{A+B} - E_A - E_B$. According to energy conservation, in particular, given that there are no body or traction forces or energy dissipation mechanisms, E_A , E_B and E_{A+B} must all be constant in time. Consequently,

$$\int \rho(\vec{R}) \vec{u}_A \cdot \vec{u}_B d^3 \vec{R} = 0 \quad (A7)$$

$$\int c_{ijkl} u_{Ai,j} u_{Bk,l} d^3 \vec{R} = 0 \quad (A8)$$

Equation (A7) appears without derivation in Hotz *et al.*³¹ It also appears without derivation as Eq. (40) of a previous work by Roca *et al.* on optical vibrational modes³² which are formally similar to the continuum acoustic phonons discussed here. Additional details are given in Appendix C.

Each of Eq. (A7) and Eq. (A8) provides an orthogonality on nondegenerate normal modes of vibrations. For convenience, we choose to orthonormalize the normal modes as in Eq. (1). Within a degenerate subspace, Gram-Schmidt orthogonalization can be used with this inner product to generate a complete orthonormal basis of normal modes.

APPENDIX B: ENERGY EQUIPARTITION

Nanoparticle vibrations are very far from thermal equilibrium when a short pulse of laser light heats the nanoparticle to thousands of degrees. Conversely, many experiments are done with low incident laser beam intensities so that temperature is constant throughout the nanoparticle and surrounding matrix.

For a linear classical mechanical system in thermodynamic equilibrium, each degree of freedom has average energy $k_B T$. Here we consider the approximate applicability of this equipartition theorem to vibrations of the embedded nanoparticle.

The nanoparticle is not an isolated system because of its mechanical connection to the matrix, but if the density or speeds of sound are significantly different (between nanoparticle and matrix) then there may be in effect a poor impedance match at the interface so that vibrational energy cannot readily enter or exit the nanoparticle. In this case there is hope that the nanoparticle can be approximated as a nearly isolated mechanical system only weakly coupled to the matrix.

Removing the matrix, the normal vibrational "pseudomodes" of the nanoparticle can be indexed by $lm\tilde{n}q$. The term "pseudomodes" emphasizes that they are not normal modes because of the non-isolation of the system. Three indices l , m and q are in common with the corresponding indices of modes of the core-shell system as a whole, \tilde{n} is the index for the nanoparticle pseudomodes and n is the index for normal modes of the entire core-shell system.

Assuming weak coupling, each pseudomode $lm\tilde{n}q$ will have average kinetic energy $\frac{1}{2}k_B T$. The coupling to the matrix leads to thermal fluctuations both of amplitude and phase of the motion within the nanoparticle. As a result the motion of a single pseudomode has a widened band of frequencies.

We add up kinetic energies within the nanoparticle for all core-shell modes whose ω_{lmnq} is close to $\omega_{lm\tilde{n}q}$ of the pseudomode. This gives a time average kinetic energy associated with the pseudomode:

$$\langle T_{lm\tilde{n}q} \rangle_t = \sum_n \frac{1}{4} \omega_{lmnq}^2 (x_{lmnq}^2 + y_{lmnq}^2) M_p \langle u_{lmnq}^2 \rangle_p \quad (B1)$$

Since each core-shell mode has average energy $k_B T$,

$x_j^2 + y_j^2$ equals $2k_B T / (M_{p+m} \omega_j^2)$. Thus,

$$\sum_n \langle u_{lmnq}^2 \rangle_p \approx \frac{M_{p+m}}{M_p} \quad (B2)$$

where the summation over n includes only such core-shell modes for which ω_{lmnq} is close to a particular pseudo-mode frequency $\omega_{lm\tilde{n}q}$.

Since normal modes are normalized with respect to Eq. (1) and since the integrand of (4) is non-negative, $\langle u_j^2 \rangle_p \leq M_{p+m} / M_p$.

APPENDIX C: GENERAL ORTHOGONALITY

It is of interest to attempt to generalize the circumstances under which the orthogonality relationships (A7) and (A8) hold, particularly because of the appearance of Eq. (A7) both in this context as well as for polar optical phonons³².

Consider a generalized elastic system which could either be a continuum elastic solid or alternatively a crystal lattice. The displacement field is \vec{u} , but \vec{u} need not merely be a 3D vector. It could be something more general such as a pair of quantities \vec{u}^+ and \vec{u}^- to represent cation and anion displacement fields in a model of optical phonons.

Suppose that the kinetic energy T is a real-valued bilinear functional $T(\vec{u}, \vec{u})$. "Bilinear" means that it is linear in each of its arguments. This includes Eq. (A1), but it could also include the kinetic energy of a polar optical mode in which the reduced mass density and $\vec{u}^+ - \vec{u}^-$ is involved³², or alternatively a summation over ions in a crystal lattice.

Next, suppose that the elastic potential energy is of the form $V(\vec{u}, \vec{u})$, where V is a real-valued bilinear functional. This is sufficiently general to allow a wide variety of continuum elasticity and elastic crystal lattice models. The only restrictions are that the forces are linear, conservative and without time delay.

In addition, suppose that there is static electric field energy U given by a space integral of $\frac{1}{2} \epsilon(\vec{R}) \|\vec{E}\|^2$ where $\epsilon(\vec{R})$ is the permittivity at the frequency of interest. Thus U is a real-valued bilinear functional $U(\vec{E}, \vec{E})$.

It is assumed that the divergence of \vec{E} is related to bound charge density, and that bound charge density is related through a linear operator to \vec{u} . This extension allows polar optical phonons as well as piezoelectric materials. Likewise \vec{E} adds a linear body force term to the equation of motion for \vec{u} , as would be the case for either polar optical phonons or a piezoelectric crystal.

It is also necessary to assume that the region over which the electric field extends is small enough that the electrostatic approximation is valid. For a polar optical mode or piezoelectric nanoparticle, the associated electric field would extend some distance into the glass matrix, but would not be large throughout the entire matrix. Typically nanoparticles are much smaller than optical wavelengths.

A given normal mode j of the equations of motion consists of a displacement field $\vec{u}_j(\vec{R})$, an electric field $\vec{E}_j(\vec{R})$ and a frequency ω_j . The argument now proceeds as in Appendix A above. Consider two non-degenerate modes A and B. The total energy E is $T(t) + U(t) + V(t)$. Since E cannot depend on time, it follows that $T(\vec{u}_A, \vec{u}_B) = 0$ which implies Eq. (A7) holds for the situation of this paper as well as for the polar optical phonons of Roca *et al.*³², thus justifying their Eq. (40).

Equation (A8) would not hold for a polar optical phonon. But it would be the case that $V(\vec{u}_A, \vec{u}_B) + U(\vec{E}_A, \vec{E}_B)$ is zero for nondegenerate normal modes A and B.

APPENDIX D: ACOUSTIC IMPEDANCE

Acoustic impedance for sound waves can be generalized to the situation of a spherical wave crossing a spherical surface at normal incidence. In this case the acoustic impedance is complex valued. In addition to density and speed of sound it also depends on frequency and the radius of the interface. When the interface radius is large compared to the wavelength the acoustic impedance again approaches density times speed of sound. See equation (5.11.12) on page 128 of L. E. Kinsler *et al.*³³

^{*} Electronic address: dmurray@ouc.bc.ca
[†] Electronic address: lucien.saviot@u-bourgogne.fr

¹ H. Lamb, Proc. London Math. Soc. **13**, 189 (1882).
² J. I. Gersten, D. A. Weitz, T. J. Gramila, and A. Z. Genack, Phys. Rev. B **22**, 4562 (1980).
³ E. Duval, A. Boukenter, and B. Champagnon, Phys. Rev. Lett **56**, 2052 (1986).
⁴ A. Li Bassi, C. E. Bottani, A. Stella, P. Tognini, P. Cheyssac, and R. Kofman, Materials Science and Engineering C **15**, 21 (2001).
⁵ M. H. Kuok, H. S. Lim, S. C. Ng, N. N. Liu, and Z. K. Wang, Phys. Rev. Lett. **90**, 255502 (2003), erratum to be published.
⁶ C. Voisin, D. Christofilos, N. Del Fatti, and F. Vallée, Physica B **316–317**, 89 (2002).
⁷ M. Gotić, M. Ivanda, A. Sekulić, S. Musić, S. Popović, A. Turković, and K. Furić, Mat. Lett. **28**, 225 (1996).
⁸ M. Ivanda, S. Musić, S. Popović, and M. Gotić, J. Mol. Struct. **480–481**, 645 (1999).
⁹ M. Ristić, M. Ivanda, S. Popović, and S. Musić, Journal of Non-Crystalline Solids **303**, 270 (2002).
¹⁰ A. Diéguez, A. Romano-Rodríguez, A. Vilá, and J. R. Morante, Journal of Applied Physics **90**, 1550 (2001).
¹¹ L. Saviot, B. Champagnon, E. Duval, I. A. Kudriavtsev, and A. I. Ekimov, Journal of Non-Crystalline Solids **197**, 238 (1996).
¹² V. A. Dubrovskiy and V. Morochnik, Earth Physics **17**, 494 (1981).
¹³ L. Saviot, D. B. Murray, and M. del C. Marco de Lucas (2003), cond-mat/0307634.
¹⁴ A. A. Sirenko, V. I. Belitsky, T. Ruf, M. Cardona, A. I. Ekimov, and C. Trallero-Giner, Phys. Rev. B **58**, 2077 (1998).
¹⁵ H. Portalès, L. Saviot, E. Duval, M. Gaudry, E. Cottancin, M. Pellarin, J. Lermé, and M. Broyer, Phys. Rev. B **65**, 165422 (2002).
¹⁶ C. W. Bettenhausen, W. C. Bowie, and M. R. Geller, Phys. Rev. B **68**, 035431 (2003).
¹⁷ T. Takagahara, Journal of Luminescence **70**, 129 (1996).
¹⁸ E. Duval, Phys. Rev. B **46**, 5795 (1992).
¹⁹ H. Portales, L. Saviot, E. Duval, M. Fujii, S. Hayashi, N. Del Fatti, and F. Vallée, J. of Chemical Physics **115**, 3444 (2001).
²⁰ R. F. S. Hearmon, in *The elastic constants of crystals and other anisotropic materials*, edited by K. H. Hellwege and A. M. Hellwege (Springer-Verlag, Berlin, 1984), no. III/18 in Landolt-Börstein Tables, p. 559.
²¹ P. Ho and A. L. Ruoff, J. Phys. Chem. Solids **29**, 2101 (1968).
²² M. Fujii, Y. Kanzawa, S. Hayashi, and K. Yamamoto, Phys. Rev. B **54**, 8373 (1996).
²³ M. Pauthe, E. Bernstein, J. Dumas, L. Saviot, A. Pradel, and M. Ribes, J. Mater. Chem. **9**, 187 (1999).
²⁴ A. Othmani, C. Bovier, J. C. Plenet, J. Dumas, B. Champagnon, and C. Mai, Materials Science and Engineering A **168**, 263 (1993).
²⁵ L. Saviot, B. Champagnon, E. Duval, and A. I. Ekimov, Phys. Rev. B **57**, 341 (1998).
²⁶ T. Tanaka, S. Onari, and T. Arai, Phys. Rev. B **47**, 1237 (1993).
²⁷ D. Berlincourt, H. Jaffe, and L. R. Shiozawa, Phys. Rev. **129**, 1009 (1963).
²⁸ A. A. Antoniou and J. A. Morrison, J. Appl. Phys. **36**, 1873 (1965).
²⁹ L. Pasquini, A. Barla, A. I. Chumakov, O. Leupold, R. Rüffer, A. Deriu, and E. Bonetti, Phys. Rev. B **66**, 073410 (2002).
³⁰ M. R. Geller, W. M. Dennis, V. A. Markel, K. R. Patton, D. T. Simon, and H.-S. Yang, Physica B **316–317**, 430 (2002), cond-mat/0107241.
³¹ R. Hotz, J. K. Krüger, W. Possart, and R. Tadros-Morgane, J. Phys.: Condens. Matter **13**, 7953 (2001).
³² E. Roca, C. Trallero-Giner, and M. Cardona, Phys. Rev. B **49**, 13704 (1994).
³³ L. E. Kinsler, A. R. Frey, A. B. Coppens, and J. V. Sanders, *Fundamentals of Acoustics* (Wiley, 2000), 4th ed.